© 2018. Published by The Company of Biologists Ltd | Development (2018) 145, dev161323. doi:10.1242/dev.161323

RESEARCH REPORT

Dynamic cytoplasmic projections connect mammalian spermatogonia *in vivo*

Bryan A. Niedenberger[1], Kenneth Cook[1], Valentina Baena[2], Nicholas D. Serra[1], Ellen K. Velte[1], Julio E. Agno[3], Karen A. Litwa[1], Mark Terasaki[2], Brian P. Hermann[4], Martin M. Matzuk[3] and Christopher B. Geyer[1,5,*]

ABSTRACT

Throughout the male reproductive lifespan, spermatogonial stem cells (SSCs) produce committed progenitors that proliferate and then remain physically connected in growing clones via short cylindrical intercellular bridges (ICBs). These ICBs, which enlarge in meiotic spermatocytes, have been demonstrated to provide a conduit for postmeiotic haploid spermatids to share sex chromosome-derived gene products. In addition to ICBs, spermatogonia exhibit multiple thin cytoplasmic projections. Here, we have explored the nature of these projections in mice and find that they are dynamic, span considerable distances from their cell body (≥25 µm), either terminate or physically connect multiple adjacent spermatogonia, and allow for sharing of macromolecules. Our results extend the current model that subsets of spermatogonia exist as isolated cells or clones, and support a model in which spermatogonia of similar developmental fates are functionally connected through a shared dynamic cytoplasm mediated by thin cytoplasmic projections.

KEY WORDS: TEX14, Intercellular bridge, Spermatogenesis, Spermatogonia, Testis, Mouse, Baboon

INTRODUCTION

The foundation of mammalian spermatogenesis is provided by continuous action of SSCs, which undergo a fate decision to either renew their population or produce transit-amplifying progenitor spermatogonia that proliferate before differentiating in response to retinoic acid (RA) and eventually entering meiosis as spermatocytes. The most widely accepted kinetic model of SSC self-renewal and differentiation in mammalian testes was first proposed in 1971, and links cell fate to spermatogonial clone length (Huckins, 1971; Oakberg, 1971). As isolated A_{single} (A_s) SSCs divide, they can produce two A_s spermatogonia or become linked via an ICB and form a clone (or chain) of A_{paired} (A_{pr}) spermatogonia. These A_{pr} spermatogonia proliferate to form longer clones of $A_{aligned}$ (A_{al}) transit-amplifying progenitors that are increasingly committed to differentiation. These original morphology-based predictions of cellular fate have been confirmed by recent fate marker, regeneration and transplantation analyses (Chan et al., 2014; Grisanti et al., 2009; Hara et al., 2014; Helsel et al., 2017).

ICBs presumably form after incomplete cytokinesis in germ cells expressing TEX14, which interacts with 'centrosomal protein 55' (CEP55) and blocks cell abscission (Greenbaum et al., 2006; Iwamori et al., 2010; Wu et al., 2003). ICBs are retained throughout the remainder of spermatogenesis, and grow wider in meiotic spermatocytes and post-meiotic spermatids to form an open ring-shaped $TEX14^+$ structure (Greenbaum et al., 2006). ICBs permit passage of X-linked macromolecules (mRNAs and proteins) between X- and Y-chromosome-bearing haploid spermatids (Braun et al., 1989; Morales et al., 2002; Ventelä et al., 2003). However, sharing of macromolecules via ICBs has not been demonstrated in spermatogonia or spermatocytes.

In addition to ICBs, scarce classical and contemporary evidence reveals mammalian spermatogonia may have greater degrees of interconnectedness. Indeed, spermatogonia are not round or ovoid, but exhibit multiple finger-like projections (Fig. 1A; Sertoli, 1877). These projections appear longer and thinner than short cylindrical ICBs, which are 1-1.5 µm wide×0.5-1 µm long (Dym and Fawcett, 1971; Weber and Russell, 1987). In recent reports, these projections are visible following immunostaining for membrane-associated proteins, although they are only mentioned briefly in one study (Abid et al., 2014; Gassei and Orwig, 2013; Grisanti et al., 2009; Nakagawa et al., 2010; Niedenberger et al., 2015; Suzuki et al., 2009; Tokuda et al., 2007).

Recent reports reveal that spermatogonia also have cellular projections in lower organisms. In locusts, male germline stem cells (GSCs) use filopodia to interact with somatic apical cells (Dorn and Dorn, 2011). In *Drosophila* testes, short microtubule-based nanotubes extend from the GSCs into the hub to facilitate ligand-receptor interactions between GSCs and terminally differentiated somatic supportive hub cells and cyst stem cells (Lin, 2002).

In this study, we provide the first detailed examination of mammalian spermatogonial cytoplasmic projections. Using a variety of approaches, we find that these projections are distinct from ICBs. Observed in spermatogonia and their precursors (prospermatogonia/gonocytes), these projections are thin dynamic cytoplasmic elements that either terminate or connect multiple adjacent and distant spermatogonia. We found that both spermatogonial cytoplasmic projections and ICBs allow the transfer of proteins between interconnected A_s spermatogonia. Taken together, these results provide clear evidence for intercellular communication between developing spermatogonia *in vivo*.

RESULTS AND DISCUSSION

Cytoplasmic projections are distinct from ICBs

Spermatogonial cytoplasmic projections were first described by Enrico Sertoli. We recently translated this work into English for the first time (Sertoli, 2018); Sertoli noted 'interesting

[1]Department of Anatomy and Cell Biology at East Carolina University, Greenville, NC 27834, USA. [2]Department of Cell Biology, University of Connecticut Health Center, Farmington, CT 06030, USA. [3]Center for Drug Discovery and Department of Pathology and Immunology, Baylor College of Medicine, Houston, TX 77030, USA. [4]Department of Biology, University of Texas at San Antonio, San Antonio, TX 78249, USA. [5]East Carolina Diabetes and Obesity Institute at East Carolina University, Greenville, NC 27834, USA.

*Author for correspondence (geyerc@ecu.edu)

C.B.G., 0000-0003-2974-3871

Received 8 November 2017; Accepted 27 June 2018

Development (2018) 145, dev161323. doi:10.1242/dev.161323

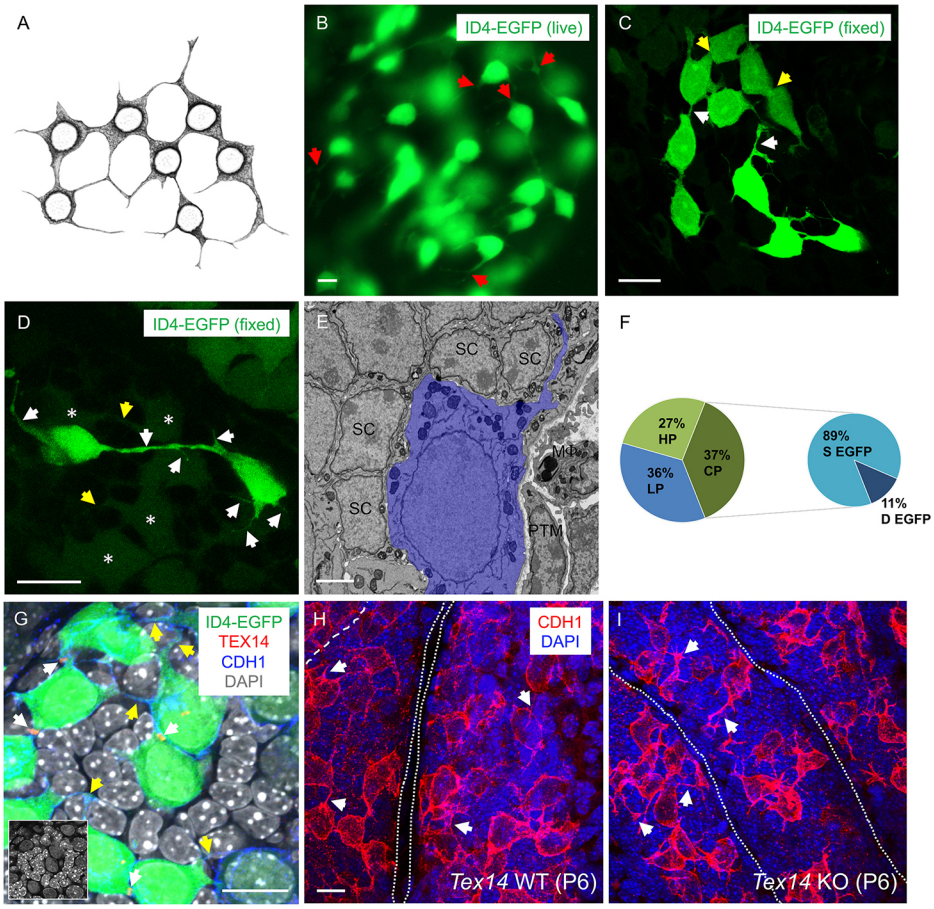

Fig. 1. Cytoplasmic projections are present in spermatogonia. (A) Scale reproduction of Sertoli's depiction of spermatogonia in fixed rat testes (Sertoli, 1877). (B) Live ID4-EGFP^{+} spermatogonia possess numerous fine, often branched, cytoplasmic projections (red arrows). (C,D) Maximum intensity projection images of whole-mounted PFA-fixed ID4-EGFP^{+} P6 testis cords. Yellow arrows in C indicate putative ICBs, while white arrows indicate cytoplasmic projections. Yellow arrows in D indicate cytoplasmic projections in ID4-EGFP^{dim} progenitor/differentiating spermatogonia (white asterisks) and white arrows indicate those in ID4-EGFP^{bright} SSCs. (E) EM showing fine projections in a P6 spermatogonium (pseudocolored blue) surrounded by Sertoli cells (SCs), peritubular myoid cells (PTMs) and macrophages (MΦs). (F) Quantitation of spermatogonia with projections and whether projections apparently connect adjacent cells of similar/dissimilar fates (Helsel et al., 2017). Twenty-seven percent have projections without clear connections (HP), 37% are connected by projections (CP) and 36% lack projections (LP). Eighty-nine percent of apparently connected cells share EGFP status (S EGFP), while 11% have differing EGFP status (D EGFP). (G) ID4-EGFP^{+} spermatogonia have TEX14^{+} ICBs (white arrows) and TEX14^{-} fine projections (yellow arrows). (H,I) CDH1^{+} undifferentiated spermatogonia in *Tex14* wild-type and KO testis cords (outlined) have similar numbers of projections (white arrows). Colored text on each image indicates immunolabeled entity. Staining carried out in triplicate from n>3 mice. Scale bars: 15 µm in B-D,G-I; 2 µm in E.

[in spermatogonia] is the presence of the projections, which give the cells their characteristic star-shaped form' (Fig. 1A) (Sertoli, 1877). These projections are visible after immunostaining whole-mounted testis cords or tubules with antibodies against membrane-associated proteins (Abid et al., 2014; Gassei and Orwig, 2013; Grisanti et al., 2009; Nakagawa et al., 2010; Niedenberger et al., 2015; Suzuki et al., 2009; Tokuda et al., 2007), although they have never been characterized.

For facile visualization of these structures, we used transgenic mice expressing enhanced green fluorescent protein (EGFP) in spermatogonia (*Id4-eGfp*; Chan et al., 2014). EGFP epifluorescence intensity is linked to spermatogonial fate in developing testes: ID4-EGFP^{bright} spermatogonia represent SSCs, whereas ID4-EGFP^{dim} and ID4-EGFP^{-} populations are progenitor and differentiating spermatogonia, respectively (Chan et al., 2014; Helsel et al., 2017).

We first examined the extensive network of cytoplasmic projections in live ID4-EGFP^{+} spermatogonia; numerous thin projections of varying lengths were straight, branched and/or had enlargements (Fig. 1B). Projections were preserved in both ID4-EGFP^{dim} and ID4-EGFP^{bright} fixed cells, and appeared to connect spermatogonia up to 30 µm apart (Fig. 1C,D). Projections were readily discerned by electron microscopy (EM), coursing between adjacent Sertoli cells (Fig. 1E). Projections were present in nearly all ID4-EGFP^{+} spermatogonia, and 58% appeared to interconnect adjacent spermatogonia. Moreover, nearly all apparently interconnected spermatogonia exhibited similar ID4-EGFP intensity (89% appeared to connect bright-bright or dim-dim, and the remaining 11% were not apparently connected, Fig. 1F), suggesting a common fate (Chan et al., 2014; Helsel et al., 2017). We expect to have underestimated the frequency and numbers of projections; those extending towards or away from the visualized plane went undetected. In addition, we likely underestimated the lengths of projections at oblique angles to the visualized plane.

Spermatogonial projections appeared too long and narrow to represent short cylindrical ICBs (Weber and Russell, 1987). We employed three approaches to discriminate between cytoplasmic projections and bona fide ICBs. First, we stained intact cords from *Id4-eGfp* testes with an antibody recognizing TEX14, an integral

Development (2018) 145, dev161323. doi:10.1242/dev.161323

component of all germ cell ICBs (Greenbaum et al., 2006; Iwamori et al., 2010). The vast majority (86%) of all cytoplasmic projections over 4 µm long were TEX14^{-}, indicating longer projections were not ICBs, even in KIT^{+} differentiating spermatogonia (Fig. 1G, Fig. S1). Second, we averaged dimensions of TEX14^{+} ICBs and TEX14^{-} cytoplasmic projections. Although sizes varied somewhat, TEX14^{+} connections were significantly (P<0.01) shorter and wider (2.8 µm×1.2 µm) than TEX14^{-} projections (8.1 µm×0.68 µm). Third, we compared cytoplasmic projections in intact testis cords from wild-type and *Tex14* KO mice by immunostaining for CDH1, which marks most spermatogonia at this stage (Niedenberger et al., 2015; Tokuda et al., 2007). *Tex14* KO mice lack ICBs (Greenbaum et al., 2006; Iwamori et al., 2010; Kim et al., 2015), yet exhibited multiple projections appearing to connect adjacent spermatogonia, as in wild-type littermates (Fig. 1H,I). Spermatogonia in *Tex14* KO testes were more likely to be apparently connected by projections (72.5% in *Tex14* KO, 57.9% in wild type, P<0.05). The average number of projections per cell did not differ between genotypes (3.4 in *Tex14* KO, 2.8 in wild type, P=0.22). Taken together, these data reveal most cytoplasmic projections, especially long thin ones, were not TEX14+ ICBs. These results highlight the necessity for researchers to determine spermatogonial clone length by staining with TEX14, rather than making assumptions based on proximity alone.

Spermatogonial projections are present in precursor prospermatogonia, in both undifferentiated and differentiating spermatogonia, but not in meiotic spermatocytes

We next assessed the temporal appearance of projections during spermatogenesis. We first stained neonatal quiescent precursor prospermatogonia (Vergouwen et al., 1991; Western et al., 2008) for GFRA1, which is expressed in all prospermatogonia at this stage (Niedenberger et al., 2015). Projections extended from, and apparently connected, adjacent postnatal day (P)1 prospermatogonia (Fig. 2A). These appeared shorter and fewer than those on spermatogonia at P6 that were undifferentiated (GFRA1^{+}, Fig. 2B,D) or differentiating (KIT^{+}, Fig. 2C,E). The apparent connectedness and numbers of projections were similar in both GFRA1^{+} and KIT^{+} spermatogonia. As models of primate SSC renewal and differentiation differ from rodents (Fayomi and Orwig, 2018), we tested whether these spermatogonial projections were also present in primates. We stained intact testis cords (containing only spermatogonia) from a juvenile baboon using anti-GFRA1 and observed projections emanating from spermatogonia (Fig. 2F). In mice, projections were not observed after the spermatogonial stage in meiotic HIST1H1T^{+} spermatocytes (Inselman et al., 2003), which are also EGFP^{+} in *Id4-eGfp* mice (Fig. 2G,H).

A tenet of the A$_s$ stem cell model is that diminution of stem cell capacity occurs with increasing length of ICB-connected spermatogonial clones (Huckins, 1971; Oakberg, 1971). As ICBs theoretically provide cytoplasmic continuity within a clone, it has been suggested that they coordinate clonal spermatogonial fate via sharing macromolecules such as RNAs and proteins. We examined this concept in *Tex14* KO mice (Fig. S2) and found that absence of ICBs only slightly altered ratios of spermatogonia that were undifferentiated (GFRA1^{+}, from ∼12% in wild type to ∼9% in KO) but not differentiating (KIT^{+}/STRA8^{+}). We speculate that, even in the absence of ICBs in *Tex14* KO mice, cytoplasmic projections coordinate proper spermatogonial proliferation and differentiation. This would explain the earlier observation that spermatogenesis in *Tex14* KO testes did not arrest until meiosis (Greenbaum et al., 2006; Sironen et al., 2011). As spermatocytes lack these projections (Fig. 2G,H), they presumably lack a means of sharing cytoplasmic contents.

Cytoplasmic projections and ICBs provide a physical connection between adjacent spermatogonia for rapid diffusion of macromolecules (such as EGFP)

We next assessed whether these thin projections could mediate cytoplasmic exchange between adjacent spermatogonia. We first used EM on over 200 serial sections from P6 testes and observed, at high resolution, apparently continuous cytoplasm connecting neighboring spermatogonia via ICBs (Fig. 3A) and cytoplasmic projections (Fig. 3B). We next used fluorescence recovery after photobleaching (FRAP) to definitively determine whether cytoplasmic projections and ICBs represented patent connections between adjacent live spermatogonia. We photobleached ID4-EGFP^{+} spermatogonia (to 10% original fluorescence) in various configurations (A$_s$, A$_{pr}$ and A$_s$ apparently connected by projections) and quantified fluorescence recovery over a short interval (<12 min, Fig. 3C). Although recovery could theoretically result from synthesis and accumulation of nascent EGFP molecules, this generally takes several hours (Kourtis and Tavernarakis, 2009). We first photobleached A$_s$ ID4-EGFP^{bright} spermatogonia exhibiting no apparent connections; they did not regain fluorescence (Fig. 3D-G,P), revealing that was indeed too short an interval for accumulation of detectable EGFP. We next photobleached individual ID4-EGFP^{bright} spermatogonia that were apparently connected to adjacent ID4-EGFP^{bright} spermatogonia via cytoplasmic projections. These A$_s$ spermatogonia (not ICB-connected) rapidly recovered ∼40% of their original fluorescence, while their non-photobleached partners lost ∼40% of their original fluorescence (Fig. 3H-K,P). Finally, we photobleached ID4-EGFP^{bright} spermatogonia in clear A$_{pr}$ configurations (connected by ICB) and found recovery was rapid (≤10 min), while the non-photobleached partner became ∼50% less intense (Fig. 3L-P). The linear kinetics of the redistribution of EGFP over this brief interval supported rapid diffusion of EGFP molecules between cells. The percentage of EGFP shared between cells formed the 'mobile fraction' (Fig. 3Q). This is the first report, to our knowledge, documenting passage of macromolecules (here, EGFP, MW ∼27 kDa) between adjacent spermatogonia.

Cytoplasmic projections are dynamic structures connecting related spermatogonia

Our current understanding of spermatogonial behavior during development is largely based on static observations using fixed tissues and isolated macromolecules. Here, we performed time-lapse imaging of live testis cords from *Id4-eGfp* mice maintained *in situ* to determine whether spermatogonial cytoplasmic projections represented static (stable) or dynamic (transient) structures. To distinguish between these possibilities, images were captured every 5 min from 15 different sites over extended incubations and combined into movie clips (see Movie 1, still images in Fig. S3). ID4-EGFP^{dim} and ID4-EGFP^{bright} spermatogonia repeatedly extended and retracted multiple projections over relatively short time periods (∼30 min) over the ∼14 h imaging period. In Movie 1, two ID4-EGFP^{bright} spermatogonia extended projections to the cord periphery (∼0-17 s, Fig. S3A), became rounded and retracted their projections (∼18-20 s, Fig. S3B), and then nearly simultaneously underwent mitosis (∼20-22 s, Fig. S3C). The newly formed spermatogonial pairs appeared to separate but then interact multiple times over the remainder of the video (∼23-41 s, Fig. S3D-F). The top pair remained ID4-EGFP^{bright},

Development (2018) 145, dev161323. doi:10.1242/dev.161323

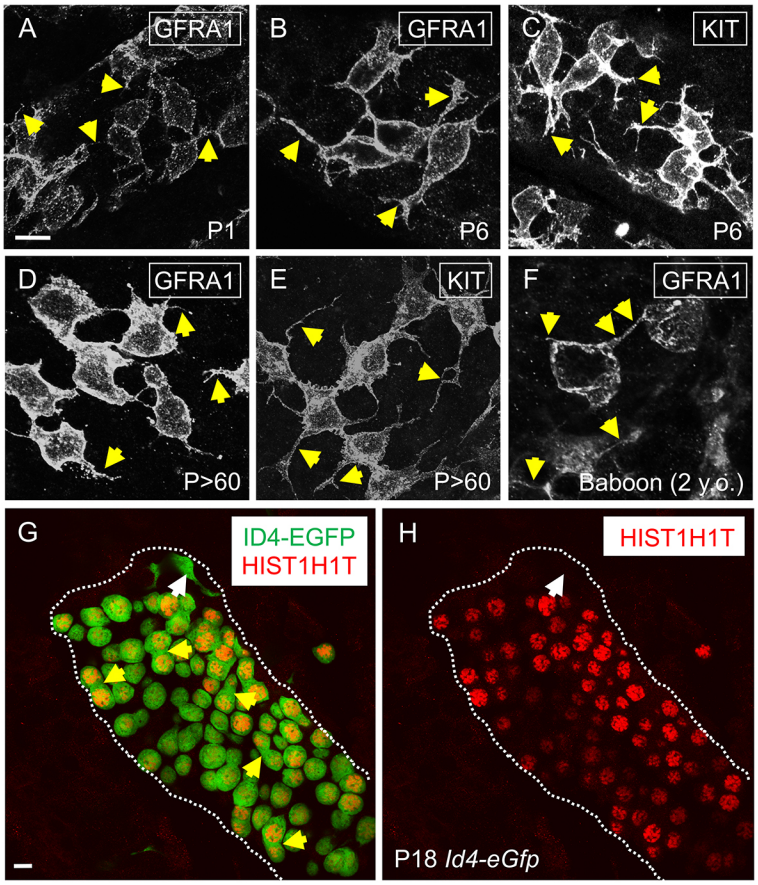

Fig. 2. Cytoplasmic projections are present in prospermatogonia as well as in undifferentiated and differentiating spermatogonia, but not in spermatocytes. Cytoplasmic projections (yellow arrows) are labeled with indicated antibodies in P1 prospermatogonia (A), P6 GFRA1$^+$ undifferentiated and KIT$^+$ differentiating spermatogonia (B,C), and adult GFRA1$^+$ and KIT$^+$ spermatogonia (D,E), as well as in GFRA1$^+$ spermatogonia from a 2-year-old baboon (F). (G,H) *Id4-eGfp* spermatocytes (HIST1H1T$^+$, red) are also EGFP$^+$, permitting visualization of cytoplasm and membranes. A lone ID4-EGFP^{bright} spermatogonium with projections is indicated by a white arrow. The seminiferous tubule is outlined and ICBs are indicated by yellow arrows. Staining was carried out in triplicate from four or more mice. Scale bars: 15 µm in A-F; 50 µm in G,H.

while the bottom pair became ID4-EGFP^{dim}, suggesting they adopted separate fates (SSC and progenitor/differentiating, respectively). In addition, numerous spermatogonia moved in and out of the viewing plane, suggesting movement along the testis cord.

Finally, we examined whether projections formed between related progeny following division or between unrelated cells. We employed Brainbow R26R-Confetti transgenic mice (JAX #013731). In this model, Cre-mediated deletions or inversions in the Brainbow transgene activate nuclear GFP (green), cytoplasmic RFP (red) or YFP (yellow), or membrane-tethered CFP (blue) (Fig. S4; Cai et al., 2013; Livet et al., 2007). We crossed Brainbow with *Ddx4*-Cre transgenic mice, which begin to express Cre recombinase in the male germline around E15 (Gallardo et al., 2007). Continuous Cre activity would cause a predicted evolution of deletions and inversions in the Brainbow transgene, creating spermatogonia singly expressing GFP, RFP, YFP or CFP or combined GFP/YFP or RFP/CFP (the latter two from repeated inversions, see Fig. S4). We found spermatogonia were either YFP$^+$, RFP$^+$, CFP$^+$ or RFP$^+$/CFP$^+$, but never GFP$^+$. According to the donating investigator (H. Clevers, Hubrecht Institute, Utrecht, the Netherlands www.jax.org), weaker Cre expression was correlated with fewer GFP$^+$ cells. Based on potential combinations from continuous inversions (Fig. S4), YFP$^+$ spermatogonia arose from different precursors than RFP$^+$, CFP$^+$ or RFP$^+$/CFP$^+$ spermatogonia. YFP$^+$/RFP$^+$ or YFP$^+$/CFP$^+$ spermatogonia would indicate sharing of fluorescent protein across projections between unrelated spermatogonia, which we never observed (Fig. 4). Therefore, we conclude that projections physically connect spermatogonia arising from common precursors. These observations resemble those from the Capel lab; only fetal prospermatogonia from wild-type×GFP chimeric mice of similar origin (WT/WT or GFP$^+$/GFP$^+$) were observed to interact via ICBs (Mork et al., 2012).

Here, we report that mammalian spermatogonia are connected by an extensive network of fine cytoplasmic projections *in vivo*. These projections are dynamic and transient, and provide patent connections between adjacent spermatogonia that, in addition to ICBs, allow for passage of macromolecules (here, EGFP) between spermatogonia of similar fates. The full functionality of these cytoplasmic projections will likely be elucidated in future studies, but we can certainly speculate on their potential *in vivo* role(s) based on known spermatogonial behavior. First, some may be precursors to ICB formation; it has been assumed, but not shown, that they form due to incomplete cytokinesis. Second, it is clear that spermatogonia move within mammalian seminiferous tubules (Hara et al., 2014; Yoshida et al., 2007), and these dynamic projections may function as filopodia to direct this movement. Third, as each spermatogonium is surrounded by numerous somatic cells, it is likely that these projections allow for ligand-receptor interactions in a similar manner to those described in *Drosophila* testes, in which MT-nanotubes relayed BMP signaling exchanges between GSCs and the nearby hub (Lin, 2002). Indeed, mammalian spermatogonial fate is regulated in large part by ligand-receptor interactions, including GDNF-GFRA1/RET, FGF-FGFR, RA-RAR/RXR and KITL-KIT (reviewed by Busada and Geyer, 2015; Mark et al., 2015; Oatley and Brinster, 2012; Yang and Oatley, 2014). Undifferentiated and differentiating spermatogonia generally express differing levels of these receptors, which poises them to respond to localized signals that direct or maintain their fate. We predict that further investigation into the specific roles played by these projections will significantly enhance our understanding of mammalian spermatogonial biology.

Development (2018) 145, dev161323. doi:10.1242/dev.161323

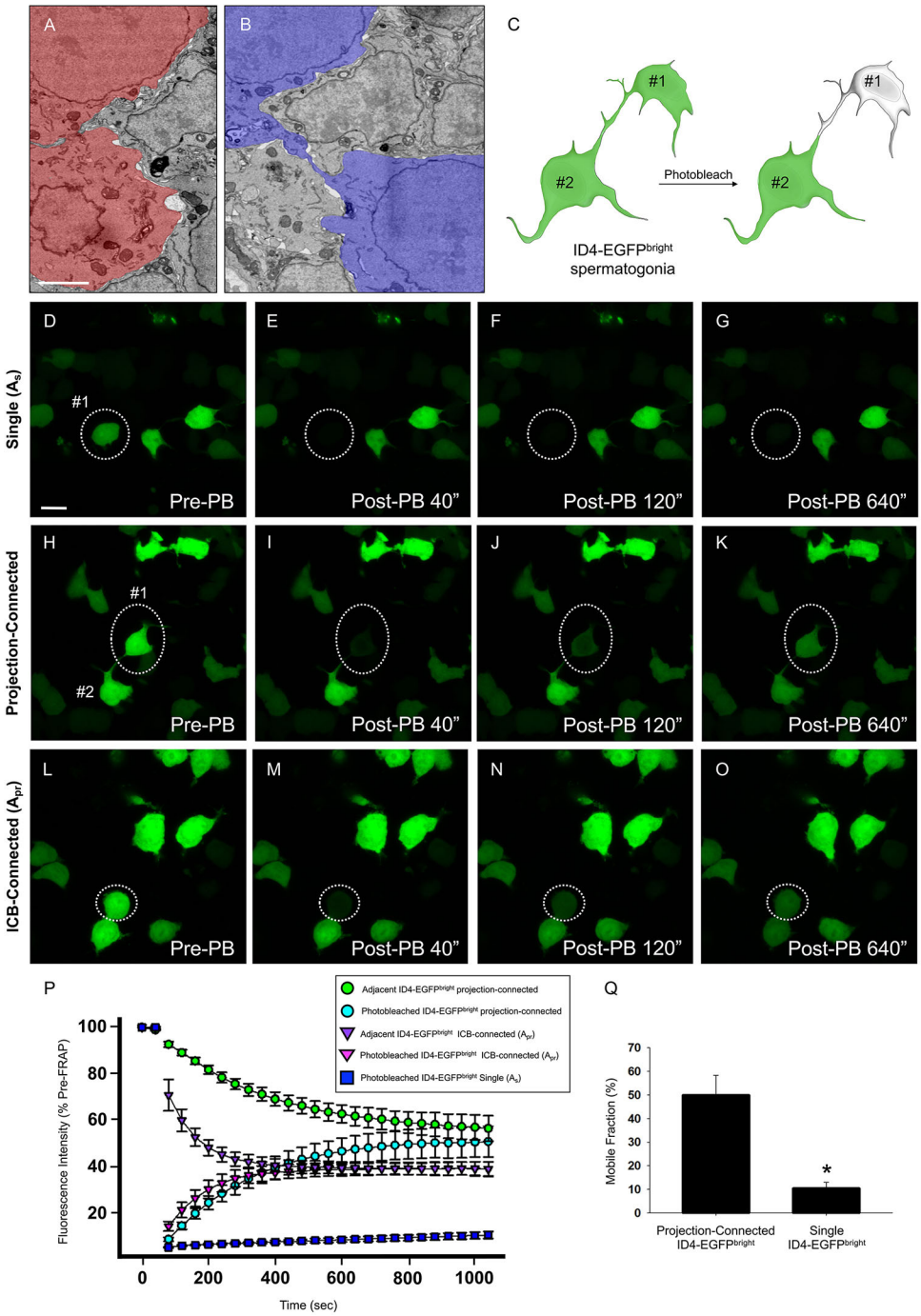

Fig. 3. Cytoplasmic projections connect adjacent spermatogonia. (A,B) Serial EM was performed on P6 testes; adjacent ICB-connected spermatogonia are pseudocolored red; those connected by a thin cytoplasmic projection are blue. (C) FRAP was carried out on adjacent spermatogonia (#1, photobleached; #2, adjacent non-photobleached). (D-O) Images from typical experiments using single (D-G), projection-connected (H-K) or ICB-connected (L-O) ID4-EGFP^{bright} spermatogonia pre-photobleaching (Pre-PB) and post-photobleaching (Post-PB). (P) Spermatogonial FRAP results shown from multiple experiments. (Q) The mobile fraction was calculated from the plateau of EGFP recovery and represents shared EGFP. Experiments were repeated more than five times (each cell type), n>10 mice. Data are mean±s.e.m. *P=0.012, Student's two-tailed t-test. Scale bars: 2 µm in A,B; 15 µm in D-O.

MATERIALS AND METHODS

Animal care

Animal procedures were approved by the Animal Care and Use Committees of East Carolina University (Assurance #A3469-01) and Baylor College of Medicine (Assurance #A3823-01). Testes were obtained by necropsy from a 29-month-old baboon at Southwest National Primate Research Center via Texas Biomedical Research Institute (Assurance #A3082-01). All procedures followed guidelines outlined in the National Research Council Guide for the Care and Use of Laboratory Animals.

Whole-mount indirect immunofluorescence

Testes were dissected and fixed in 4% paraformaldehyde in 1×PBS at 4°C for 2 h to overnight, depending on age. After an overnight soak in 1×PBS at 4°C, testes were cut into ∼1 mm^3 pieces, permeabilized by incubation in 0.1% Triton X-100 for 30 min at room temperature, and then blocked for 1 h at room temperature with 3% BSA in 0.1% Triton X-100 in 1×PBS. Primary antibodies were diluted with 3% BSA in 0.1% Triton X-100 in 1×PBS and incubated with tissues overnight at 4°C. Tissues were then washed three times for 30 min each in 1×PBS containing 0.1% Triton X-100. Fluorescently conjugated secondary antibodies and phalloidin (to visualize F-actin) were diluted with 3% BSA in 0.1% Triton X-100 in 1×PBS, then incubated with tissue overnight at 4°C. Tissues were then washed three times for 30 min each in 0.1% Triton X-100 in 1×PBS. Tissues were mounted in Fluoroshield with DAPI (Abcam) and imaged on an Olympus FV1000 confocal microscope. Multiple z-stacked images were acquired (10 when using the 60× objective, five when using the 60× objective with 2× digital zoom) that were 2 µm apart, and merged in ImageJ to generate maximum intensity projections. Details for primary antibodies and labeling reagents are provided in Table S1.

Development (2018) 145, dev161323. doi:10.1242/dev.161323

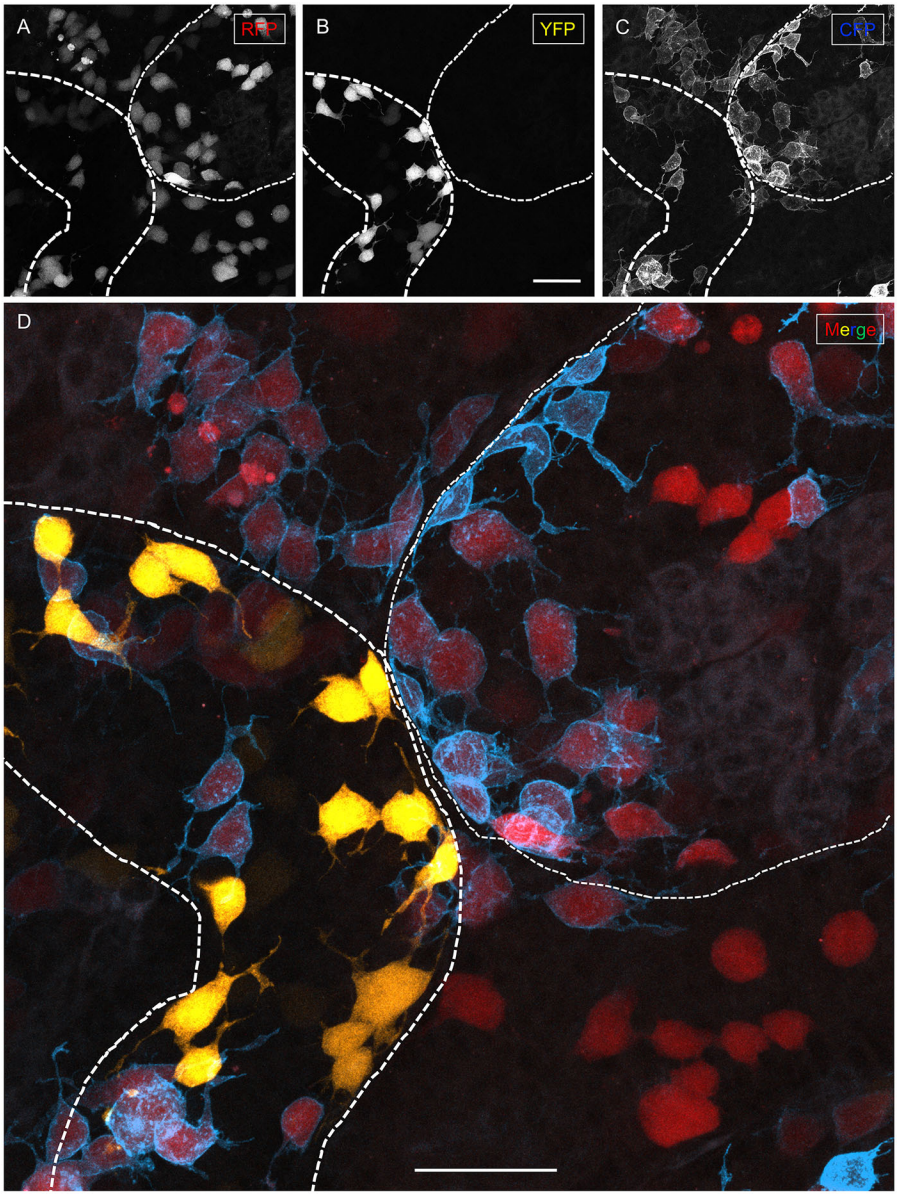

Fig. 4. Cytoplasmic projections do not connect unrelated spermatogonia. (A-D) Maximum intensity projection from R26R-Confetti;*Ddx4*-Cre testes shown with separate channels (A-C) and combined in a merged image (D). Triplicate technical replicates from *n*=2 mice from two litters. Scale bars: 50 µm.

Images used for quantitation were five-slice maximum intensity projections taken with the 60× objective with 2× digital zoom. Nine images were taken totaling 79 projections from *n*=4 mice. These projections were measured in Adobe Photoshop using an image-calibrated ruler tool. Between 6-13 projections were measured from each image.

Images of whole-mount testis cords and tubules were captured using an Olympus FluoView FV1000 confocal laser scanning microscope or a Zeiss LSM 880 with Airyscan. The determination of cells staining positive or negative for markers such as KIT and GFRA1 were performed using ImageJ software, with thresholds set at 195-255 for $ID4^{+}$ cells and 40-200 for $ID4^{-}$ cells. Nonspecific staining was removed from images of TEX14-stained sections in ImageJ with the Particle Remover tool with the threshold set to 55-255. Size was set to 0.0-0.7 µm^2 and holes were included. The Subtract Background tool was used to reduce background with rolling ball radii set to 10 pixels.

Two transgenic mice were used in the Brainbow experiments, from different litters. PFA-fixed testes were cut into ∼2 mm^3 pieces, mounted on a slide with Vectastain containing DAPI, and imaged using a 40× objective. Images consisted of two stacks with 43-68 1 µm slices. Each slice was carefully examined for connected cells to determine whether spermatogonia expressing different fluorophore combinations were connected by projections. *Z*-stack images were captured on the Olympus FV-1000 as well as the Zeiss LSM 880 with Airyscan. Time-lapse experiments were repeated 15 times (15 movies were recorded) in two separate experiments using testes from eight different *Id4-eGfp* mice. FRAP experiments were repeated five times for each type of cell type (A_s, ICB-connected A_{pr} and projection-connected) on at least 10 mice.

Serial electron microscopy

Whole testes were incubated in 2% glutaraldehyde for 1 h at 4°C. Epididymides were removed and testes cut into several pieces. Fixation was carried out in 2% glutaraldehyde overnight at 4°C, followed by three successive washes in 0.1 M cacodylate buffer. For wild-type testes, post-fixation was performed in 1% osmium tetroxide at room temperature for 1 h, followed by three 15 min washes with sodium phosphate buffer. Testes were then dehydrated through a graded ethanol series (25%, 50%, 70%, 95%, 100%) at room temperature. Following fixation, testes were embedded in Spurr's medium (Electron Microscopy Sciences) in flat tissue tear-away containers that were baked overnight at 70°C. Serial sections were captured using a tape-collecting device coupled with an ultramicrotome (Kasthuri et al., 2015). A consecutive series of 237 sections was cut at a thickness of 40 nm and collected on Kapton tape. The sections were imaged using the backscatter mode of a Zeiss Sigma field emission scanning electron microscope as previously described (Terasaki et al., 2013). A 61 µm^2 area

Development (2018) 145, dev161323. doi:10.1242/dev.161323

was imaged at a resolution of 5 nm/pixel (12,233×12,233 pixels). Images were aligned using the Linear Stack Alignment with SIFT algorithm in ImageJ.

Fluorescence recovery after photobleaching

Testes were dissected from P6 *Id4-eGfp* mice, detunicated and transferred to a glass-bottomed Petri dish. Testis cords were gently teased apart using a pair of 30-gauge needles, then covered with a slab of agarose dissolved in Fluorobrite DMEM supplemented with 4 mM L-glutamine (Thermo Fisher Scientific). All imaging was performed at 37°C with 5% CO_2 in a humid chamber on an Olympus FV1000 confocal microscope equipped with Olympus Fluoview software. FRAP imaging was performed with the following parameters: (*z*-stack, four slices of 2 µm each), 2% laser intensity, 800×800 pixels, 4 µs/pixel scan speed and a fully-open aperture. Photobleaching was carried out with 100% laser intensity at 100 µs/pixel. Specimens were imaged 80 and 40 s prior to photobleaching, and then a total of 25 times every 40 s after photobleaching.

Measurements of fluorescence intensity were carried out in ImageJ with Time Series Analyzer V3.0. The intensity was normalized at each timepoint using Microsoft Excel with the following steps: (1) we subtracted the average intensity of the background (a dark area with no visible cells) from the average intensity from a non-photobleached cell; (2) the resulting value for each time point was then divided by the resulting value for the initial timepoint; (3) the average background intensity over the course of the experiment was then subtracted from the average intensity of a frapped cell for each timepoint; (4) the resulting number [calculated in (3)] was then divided by the number calculated in (2) and (5). The result of (4) for each timepoint was divided by (4) at the initial timepoint, then multiplied by 100 to calculate percentage change in average intensity, which was then analyzed using Sigma Plot 13.0.

Time-lapse live imaging

Tissues were mounted as above for FRAP, and imaged at 37°C with 5% CO_2 in a humid chamber on a Zeiss LSM 700 laser scanning confocal microscope equipped with Zeiss Zen Black software using the 40× objective. Five *z*-stacked images were acquired with spacing of 2 µm every 5 min for a total of 14 h. This experiment was performed twice, and a total of 15 different sites were imaged. Maximum intensity projections were generated using Zen Black, and sequential images were combined to produce a short video clip.

Statistics

Statistical analyses were carried out using Student's *t*-test, and significance was set at $P<0.05$. Statistical analyses of FRAP data was performed using Sigma Plot 13.0, which determined that data assumed a normalized distribution (Shapiro-Wilk, $P=0.372$) and equal variance (Brown-Forsythe, $P=0.282$). Statistical significance was determined using a two-tailed *t*-test.

Acknowledgements

We thank Dr Jon Oatley (Washington State University, Pullman, WA, USA) for Id4-eGfp mice, Dr Eva Johannes (North Carolina State University, Raleigh, NC, USA) for technical assistance with microscopy, and Ms Katya Harris (graduate student, East Carolina University School of Art and Design, Greenville, NC, USA) for illustrations.

Competing interests

The authors declare no competing or financial interests.

Author contributions

Conceptualization: N.D.S., K.A.L., M.T., B.P.H., C.B.G.; Methodology: B.A.N., E.K.V., J.E.A., K.A.L., M.T., C.B.G.; Software: C.B.G.; Validation: C.B.G.; Formal analysis: B.A.N., E.K.V., K.A.L., C.B.G.; Investigation: B.A.N., K.C., V.B., N.D.S., C.B.G.; Resources: J.E.A., M.T., B.P.H., M.M.M., C.B.G.; Data curation: C.B.G.; Writing - original draft: B.A.N., C.B.G.; Writing - review & editing: M.T., B.P.H., M.M.M., C.B.G.; Visualization: C.B.G.; Supervision: C.B.G.; Project administration: C.B.G.; Funding acquisition: B.P.H., M.M.M., C.B.G.

Funding

Research was supported by grants from the Eunice Kennedy Shriver National Institute of Child Health and Human Development (1R01HD090083 to C.B.G. and P01HD087157 to M.M.M.). This investigation used resources supported by the Southwest National Primate Research Center grant (P51 OD011133) from the National Institutes of Health's Office of Research Infrastructure Programs. Deposited in PMC for release after 12 months.

Supplementary information

Supplementary information available online at
http://dev.biologists.org/lookup/doi/10.1242/dev.161323.supplemental

References

Abid, S. N., Richardson, T. E., Powell, H. M., Jaichander, P., Chaudhary, J., Chapman, K. M. and Hamra, F. K. (2014). A-single spermatogonia heterogeneity and cell cycles synchronize with rat seminiferous epithelium stages VIII-IX. *Biol. Reprod.* **90**, 32.

Braun, R. E., Behringer, R. R., Peschon, J. J., Brinster, R. L. and Palmiter, R. D. (1989). Genetically haploid spermatids are phenotypically diploid. *Nature* **337**, 373-376.

Busada, J. T. and Geyer, C. B. (2015). The role of retinoic acid (RA) in spermatogonial differentiation. *Biol. Reprod.* **94**, 10.

Cai, D., Cohen, K. B., Luo, T., Lichtman, J. W. and Sanes, J. R. (2013). Improved tools for the Brainbow toolbox. *Nat. Methods* **10**, 540-547.

Chan, F., Oatley, M. J., Kaucher, A. V., Yang, Q. E., Bieberich, C. J., Shashikant, C. S. and Oatley, J. M. (2014). Functional and molecular features of the Id4+ germline stem cell population in mouse testes. *Genes Dev.* **28**, 1351-1362.

Dorn, D. C. and Dorn, A. (2011). Structural characterization and primary in vitro cell culture of locust male germline stem cells and their niche. *Stem Cell Res.* **6**, 112-128.

Dym, M. and Fawcett, D. W. (1971). Further observations on the numbers of spermatogonia, spermatocytes, and spermatids connected by intercellular bridges in the mammalian testis. *Biol. Reprod.* **4**, 195-215.

Fayomi, A. P. and Orwig, K. E. (2018). Spermatogonial stem cells and spermatogenesis in mice, monkeys and men. *Stem Cell Res.* **29**, 207-214.

Gallardo, T., Shirley, L., John, G. B. and Castrillon, D. H. (2007). Generation of a germ cell-specific mouse transgenic Cre line, Vasa-Cre. *Genesis* **45**, 413-417.

Gassei, K. and Orwig, K. E. (2013). SALL4 expression in gonocytes and spermatogonial clones of postnatal mouse testes. *PLoS ONE* **8**, e53976.

Greenbaum, M. P., Yan, W., Wu, M.-H., Lin, Y.-N., Agno, J. E., Sharma, M., Braun, R. E., Rajkovic, A. and Matzuk, M. M. (2006). TEX14 is essential for intercellular bridges and fertility in male mice. *Proc. Natl. Acad. Sci. USA* **103**, 4982-4987.

Grisanti, L., Falciatori, I., Grasso, M., Dovere, L., Fera, S., Muciaccia, B., Fuso, A., Berno, V., Boitani, C., Stefanini, M. et al. (2009). Identification of spermatogonial stem cell subsets by morphological analysis and prospective isolation. *Stem Cells* **27**, 3043-3052.

Hara, K., Nakagawa, T., Enomoto, H., Suzuki, M., Yamamoto, M., Simons, B. D. and Yoshida, S. (2014). Mouse spermatogenic stem cells continually interconvert between equipotent singly isolated and syncytial states. *Cell Stem Cell* **14**, 658-672.

Helsel, A. R., Yang, Q.-E., Oatley, M. J., Lord, T., Sablitzky, F. and Oatley, J. M. (2017). ID4 levels dictate the stem cell state in mouse spermatogonia. *Development* **144**, 624-634.

Huckins, C. (1971). The spermatogonial stem cell population in adult rats. I. Their morphology, proliferation and maturation. *Anat. Rec.* **169**, 533-557.

Inselman, A., Eaker, S. and Handel, M. A. (2003). Temporal expression of cell cycle-related proteins during spermatogenesis: establishing a timeline for onset of the meiotic divisions. *Cytogenet Genome Res.* **103**, 277-284.

Iwamori, T., Iwamori, N., Ma, L., Edson, M. A., Greenbaum, M. P. and Matzuk, M. M. (2010). TEX14 interacts with CEP55 to block cell abscission. *Mol. Cell. Biol.* 30, 2280-2292.

Kasthuri, N., Hayworth, K. J., Berger, D. R., Schalek, R. L., Conchello, J. A., Knowles-Barley, S., Lee, D., Vazquez-Reina, A., Kaynig, V., Jones, T. R. et al. (2015). saturated reconstruction of a volume of neocortex. *Cell* **162**, 648-661.

Kim, H. J., Yoon, J., Matsuura, A., Na, J.-H., Lee, W.-K., Kim, H., Choi, J. W., Park, J. E., Park, S.-J., Kim, K. T. et al. (2015). Structural and biochemical insights into the role of testis-expressed gene 14 (TEX14) in forming the stable intercellular bridges of germ cells. *Proc. Natl. Acad. Sci. USA* **112**, 12372-12377.

Kourtis, N. and Tavernarakis, N. (2009). Cell-specific monitoring of protein synthesis in vivo. *PLoS ONE* **4**, e4547.

Lin, H. (2002). The stem-cell niche theory: lessons from flies. *Nat. Rev. Genet.* **3**, 931-940.

Livet, J., Weissman, T. A., Kang, H., Draft, R. W., Lu, J., Bennis, R. A., Sanes, J. R. and Lichtman, J. W. (2007). Transgenic strategies for combinatorial expression of fluorescent proteins in the nervous system. *Nature* **450**, 56-62.

Mark, M., Teletin, M., Vernet, N. and Ghyselinck, N. B. (2015). Role of retinoic acid receptor (RAR) signaling in post-natal male germ cell differentiation. *Biochim. Biophys. Acta* **1849**, 84-93.

Morales, C. R., Lefrancois, S., Chennathukuzhi, V., El-Alfy, M., Wu, X., Yang, J., Gerton, G. L. and Hecht, N. B. (2002). A TB-RBP and Ter ATPase complex

accompanies specific mRNAs from nuclei through the nuclear pores and into intercellular bridges in mouse male germ cells. *Dev. Biol.* **246**, 480-494.
Mork, L., Tang, H., Batchvarov, I. and Capel, B. (2012). Mouse germ cell clusters form by aggregation as well as clonal divisions. *Mech. Dev.* **128**, 591-596.
Nakagawa, T., Sharma, M., Nabeshima, Y., Braun, R. E. and Yoshida, S. (2010). Functional hierarchy and reversibility within the murine spermatogenic stem cell compartment. *Science* **328**, 62-67.
Niedenberger, B. A., Busada, J. T. and Geyer, C. B. (2015). Marker expression reveals heterogeneity of spermatogonia in the neonatal mouse testis. *Reproduction* **149**, 329-338.
Oakberg, E. F. (1971). Spermatogonial stem-cell renewal in the mouse. *Anat. Rec.* **169**, 515-531.
Oatley, J. M. and Brinster, R. L. (2012). The germline stem cell niche unit in mammalian testes. *Physiol. Rev.* **92**, 577-595.
Sertoli, E. (1877). Sulla struttura dei canalicoli seminiferi dei testicoli studiata in rapport allo svillupo dei nemaspermi. *Archivo per le Scienze Mediche* **2**, 267-295.
Sertoli, E. (2018). The structure of seminiferous tubules and the development of [spermatids] in rats. *Biol. Reprod.* ioy134. doi: 10.1093/biolre/ioy134.
Sironen, A., Uimari, P., Venhoranta, H., Andersson, M. and Vilkki, J. (2011). An exonic insertion within Tex14 gene causes spermatogenic arrest in pigs. *BMC Genomics* **12**, 591.
Suzuki, H., Sada, A., Yoshida, S. and Saga, Y. (2009). The heterogeneity of spermatogonia is revealed by their topology and expression of marker proteins including the germ cell-specific proteins Nanos2 and Nanos3. *Dev. Biol.* **336**, 222-231.
Terasaki, M., Shemesh, T., Kasthuri, N., Klemm, R. W., Schalek, R., Hayworth, K. J., Hand, A. R., Yankova, M., Huber, G., Lichtman, J. W. et al. (2013). Stacked endoplasmic reticulum sheets are connected by helicoidal membrane motifs. *Cell* **154**, 285-296.
Tokuda, M., Kadokawa, Y., Kurahashi, H. and Marunouchi, T. (2007). CDH1 is a specific marker for undifferentiated spermatogonia in mouse testes. *Biol. Reprod.* **76**, 130-141.
Ventelä, S., Toppari, J. and Parvinen, M. (2003). Intercellular organelle traffic through cytoplasmic bridges in early spermatids of the rat: mechanisms of haploid gene product sharing. *Mol. Biol. Cell* **14**, 2768-2780.
Vergouwen, R. P. F. A., Jacobs, S. G. P. M., Huiskamp, R., Davids, J. A. G. and de Rooij, D. G. (1991). Proliferative activity of gonocytes, Sertoli cells and interstitial cells during testicular development in mice. *J. Reprod. Fertil.* **93**, 233-243.
Weber, J. E. and Russell, L. D. (1987). A study of intercellular bridges during spermatogenesis in the rat. *Am. J. Anat.* **180**, 1-24.
Western, P. S., Miles, D. C., van den Bergen, J. A., Burton, M. and Sinclair, A. H. (2008). Dynamic regualtion of mitotic arrest in fetal male germ cells. *Stem Cells* **26**, 339-347.
Wu, M.-H., Rajkovic, A., Burns, K. H., Yan, W., Lin, Y.-N. and Matzuk, M. M. (2003). Sequence and expression of testis-expressed gene 14 (Tex14): a gene encoding a protein kinase preferentially expressed during spermatogenesis. *Gene Expr. Patterns* **3**, 231-236.
Yang, Q.-E. and Oatley, J. M. (2014). Spermatogonial stem cell functions in physiological and pathological conditions. *Curr. Top. Dev. Biol.* **107**, 235-267.
Yoshida, S., Sukeno, M. and Nabeshima, Y. (2007). A vasculature-associated niche for undifferentiated spermatogonia in the mouse testis. *Science* **317**, 1722-1726.